Generative Adversarial Networks as an Advanced Data Augmentation Technique for MRI Data

Filippos Konidaris, Thanos Tagaris, Maria Sdraka and Andreas Stafylopatis

School of Electrical and Computer Engineering, National Technical University of Athens,
Iroon Polytexneiou 9, Zografou Campus 15780, Athens, Greece

Keywords: Generative Adversarial Networks, Deep Learning, MRI, Data Augmentation, ADNI, Alzheimer's Disease.

Abstract: This paper presents a new methodology for data augmentation through the use of Generative Adversarial Networks. Traditional augmentation strategies are severely limited, especially in tasks where the images follow strict standards, as is the case in medical datasets. Experiments conducted on the ADNI dataset prove that augmentation through GANs outperforms traditional methods by a large margin, based both on the validation accuracy and the models' generalization capability on a holdout test set. Although traditional data augmentation did not seem to aid the classification process in any way, by adding GAN-based augmentation an increase of 11.68% in accuracy was achieved. Furthermore, by combining traditional with GAN-based augmentation schemes, even higher accuracies can be reached.

1 INTRODUCTION

Over the past years, there has been a rapid development in the field of Computer Vision, especially through techniques involving Deep Learning. A trend has emerged, where models achieving state-of-the-art performances are becoming deeper and more complex. An explanation might be that the most important benchmark each new Deep Neural Network must pass is the annual ImageNet Large Scale Visual Recognition Challenge (ILVRC) (Russakovsky et al., 2015), which requires the models to be trained on an immensely large dataset (i.e. millions of images). However, performance on this challenge does not always translate well to real world applications, as they rarely include such a large dataset.

Training a deep model on insufficient data usually results in overfitting, because a model of high capacity is capable of "memorizing" the training set. Multiple methods have been shown to alleviate this problem, but none so effectively to be used exclusively. These techniques can be split into two broad categories: regularization techniques, aiming to limit the model's capacity (e.g. dropout, parameter norm penalties) and data augmentation techniques, attempting to increase the size of the dataset (Kukačka et al., 2018). In practice, most models benefit from a mul-

Github repo: https://github.com/filippos1994/Gan mri aug

titude of these techniques. This study mostly focuses on the latter category.

Data augmentation has proven to be very effective and is adopted universally in the field of deep learning, e.g. (Ciresan et al., 2010), (Vasconcelos and Vasconcelos, 2017). It is in fact so effective that it is being used even in tasks that involve large amounts of data (Wu et al., 2015). The most common forms of augmentation include horizontal and vertical flips, affine transformations (e.g. scaling, translating, rotating), brightness/contrast adjustments and filter applications (e.g. blurring, sharpening). The goal of such transformations is to obtain a new image that contains the same semantic information as the original.

While augmentation most certainly helps neural networks learn and generalize more effectively, it also has its drawbacks. In most cases, augmentation techniques are limited to minor changes on an image, as more "heavy" augmentations might damage the image's semantic content. Furthermore, the forms of augmentation one can use differ from problem to problem, making their application ad-hoc and empirical. For instance, medical images have to be mildly augmented as they follow strict standards (i.e. they are centered, their orientation and intensity vary little from image to image and many times they are laterally/horizontally asymmetric) (Hussain et al., 2017). Finally, augmentation techniques are applied on one image at a time and thus are unable to gather any

information from the rest of the dataset. This paper proposes a novel technique that overcomes said limitations and is capable of augmenting any given dataset with realistic, high-quality images generated from scratch.

Generative Adversarial Networks (GANs) (Goodfellow et al., 2014) are a family of unsupervised neural networks most commonly used for image generation. Each GAN is composed of two networks: a generator and a discriminator, competing against each other in a two-player minimax game. These models have proven to be capable of creating realistic images and will serve as the basis of this study.

2 RELATED WORK

Generative Adversarial Networks have been successfully used in the past for data augmentation. For example, (Antoniou et al., 2017) and (Wang et al., 2018) use custom GAN architectures in a low-data setting achieving consistently better results than traditionally augmented classifiers, while (Perez and Wang, 2017) devise a novel pipeline called Neural Augmentation which, through style transfer techniques, aims at generating images of different styles, performing equally as good as traditional augmentation schemes in a subsequent classification task. Additionally, (Neff, 2018) proposes a generative model which learns to produce pairs of images and their respective segmentation masks in order to assist a U-Net segmentation model, proving that in simpler datasets networks trained with a mix of synthetic and real images stay competitive with networks trained on strictly real data using standard data augmentation.

One field in which data augmentation is especially important is that of medical imaging, where the lack of available public data is a ubiquitous problem since access to individual medical records is heavily protected by legislation and appropriate consent must be given. In most cases this process is hindered by bureaucracy and/or high costs, while the resulting collection is greatly imbalanced towards normal subjects. Several authors employ Machine Learning techniques to learn directly from the available data and surpass the state-of-the art in problems as diverse as generating benchmark data, image normalization, super resolution, or cross-modality synthesis (Frangi et al., 2018).

The medical field has only recently started adopting GAN-based methodologies for synthesizing images (Yi et al., 2018). In particular (Bentaieb and Hamarneh, 2018) and (Shaban et al., 2018) propose GAN-based style transfer approaches to stain nor-

malization in histopathology images, with quite interesting results in various datasets. For tackling segmentation tasks, various authors have proposed custom GAN architectures and pipelines which are adversarially trained to produce proper segmentation masks from a given medical image dataset (Shin et al., 2018), (Dai et al., 2017), (Xue et al., 2017). Regarding image translation between modes, (Dar et al., 2018) synthesize T2-weighted brain MRI images from T1-weighted ones, and vice versa, using a Conditional GAN model. Finally, many authors, such as (Frid-Adar et al., 2018) and (Costa et al., 2018), have attempted to generate counterfeit medical images in order to increase the size of the training set of different deep learning models, a task more closely related to the one examined in this paper.

Supplementary to all of the above efforts, our approach aims to exploit the superior performance of GANs for the benefit of medical image classification. We explore the impact of GAN-assisted data augmentation on the diagnosis of Alzheimer's Disease through non-invasive MRI scans and our critic is a robust CNN model designed to classify among Alzheimer's patients and healthy controls.

3 GENERATIVE ADVERSARIAL NETWORKS

A Generative Adversarial Network is composed of two networks, the generator and the discriminator. The generator accepts a noise vector as input and produces fake data, which are then fed, along with real ones, to the discriminator, whose goal is to distinguish which distribution the samples originate from. Conversely, the generator's goal is to learn the real distribution without witnessing it, in order to make its output indistinguishable from real samples. Both networks are trained simultaneously and adversarially, until an equilibrium is reached.

In order to combat instability issues during training, the Earth Mover's or Wasserstein distance was used, partially because it leads to convergence for a much broader set of distributions, but mostly because its value is directly correlated to the quality of the generated data. (Arjovsky et al., 2017). The resulting formulation of the game is presented in eq. (1), where $\mathcal{D}$ is the set of 1-Lipschitz functions.

$$\min_{G} \max_{D \in \mathcal{D}} \mathbb{E}_{\mathbf{x} \sim \mathbb{P}_r}[D(\mathbf{x})] - \mathbb{E}_{\mathbf{z} \sim \mathbb{P}_z}[D(G(\mathbf{z}))] \qquad (1)$$

The discriminator's 1-Lipschitz constraint was initially achieved by clipping its weights by an arbitrary value (WGAN). It was later shown that this

technique led to sub-optimal behaviour, which could be ameliorated with the inclusion of a gradient penalty term to the discriminator's loss function, as shown in eq. (2), calculated on a random interpolation point between the real and the fake samples ($\mathbb{P}_{\hat{x}}$) (Gulrajani et al., 2017). The resulting architecture (WGAN-GP) is the one used in the current work.

$$L = \mathbb{E}_{\mathbf{z} \sim \mathbb{P}_z}[D(G(\mathbf{z}))] - \mathbb{E}_{\mathbf{x} \sim \mathbb{P}_r}[D(\mathbf{x})] +$$
$$+ \lambda \underset{\hat{x} \sim \mathbb{P}_{\hat{x}}}{\mathbb{E}} [(\|\nabla_{\hat{x}} D(\hat{x})\|_2 - 1)^2] \quad (2)$$

4 PROPOSED AUGMENTATION METHODOLOGY

The main goal of this study was to produce realistic images for each of the classes on-demand. To achieve this, a framework was designed where a single GAN was trained on each of the classes. For this purpose, a GAN architecture of sufficient capacity to understand and model the underlying distributions of each of the classes had to be selected. A GAN that satisfies the above goal should, after training, be able to produce realistic images of the class it was trained upon.

4.1 Generator

An architecture with 11 layers and more than 15 million trainable parameters was selected as the generator of the network. The architecture is depicted in Figure 1.

The input of the generator is a vector of 128 random values in the $[0,1)$ range, sampled from a uniform distribution. Following the input is a Fully Connected (FC) layer with $6 \cdot 5 \cdot 512 = 15360$ neurons. The output of the FC layer is then transformed into a 3D volume, which can be thought of as a 6×5 image with 512 channels. The subsequent layers are regular 2D convolutions (Conv) and 2D transposed convolutions (Conv trans_up), sometimes referred to as "deconvolution" layers. A 5×5 sized kernel and 'same' padding were selected for both types of layers, while a stride of 2 was selected for the transposed convolutions. This results in the doubling of the spatial dimensions of its input.

All layers apart from the last are activated by a "Leaky ReLU" function. The final layer has a hyperbolic tangent (tanh) activation function, because its output needs to be bounded in order to be able to output an image. A tanh function was preferred over a sigmoid function because it is centered around 0, which helps during training (LeCun et al., 1998).

Finally, after five alternations of convolution and transposed convolution layers (each of which doubles
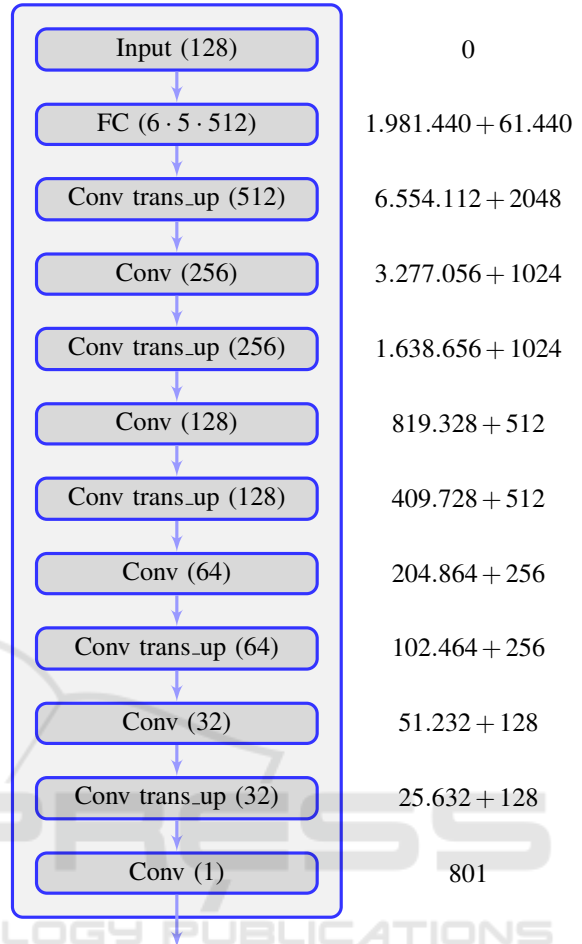

Layer	Parameters
Input (128)	0
FC ($6 \cdot 5 \cdot 512$)	$1.981.440 + 61.440$
Conv trans_up (512)	$6.554.112 + 2048$
Conv (256)	$3.277.056 + 1024$
Conv trans_up (256)	$1.638.656 + 1024$
Conv (128)	$819.328 + 512$
Conv trans_up (128)	$409.728 + 512$
Conv (64)	$204.864 + 256$
Conv trans_up (64)	$102.464 + 256$
Conv (32)	$51.232 + 128$
Conv trans_up (32)	$25.632 + 128$
Conv (1)	801

Figure 1: On the left is the architecture of the network's generator. The size of each layer can be seen after its name. On the right, the number of parameters (trainable + batch normalization) of each layer is presented.

the size of its input), an image with a resolution of $(6 \cdot 2^5 \times 5 \cdot 2^5) = (192 \times 160)$ and 1 channel is produced.

4.2 Discriminator

The discriminator is a regular CNN architecture aimed towards binary classification. The one used in the present study consists of 11 layers and around 9.5 million trainable parameters and can be seen in Figure 2.

The input to the discriminator is a single-channel 192×160 image. This image is then passed five times through alternating layers of convolutions with a stride of 1 and 2 respectively; the latter are used for sub-sampling as there are no pooling layers present in the architecture. The final two layers are FC ones. All layers in the network are activated by a "Leaky ReLU", besides the last one which has no activation function.

(192, 160, 1)

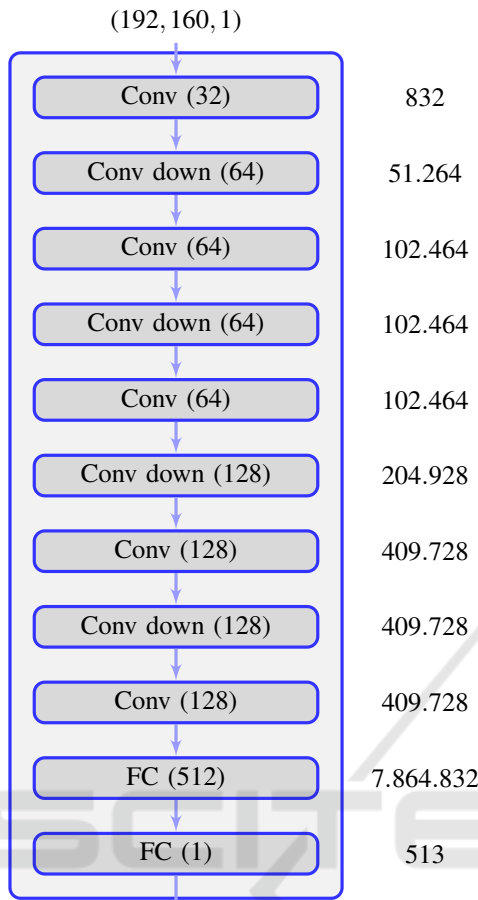|	
Conv (32)	832
Conv down (64)	51.264
Conv (64)	102.464
Conv down (64)	102.464
Conv (64)	102.464
Conv down (128)	204.928
Conv (128)	409.728
Conv down (128)	409.728
Conv (128)	409.728
FC (512)	7.864.832
FC (1)	513

Figure 2: The architecture of the network's discriminator is depicted on the left. The size of each layer can be seen after its name. The number of parameters of each layer is presented on the right of the Figure.

5 APPLICATION

For an experimental validation of the effectiveness of the proposed methodology, an application was selected where traditional augmentation techniques were ineffective. One of the most troublesome domains for data augmentation is medical imaging, since biological constraints pose great limitations on the visual transformations that can be applied without damaging the semantic content of the data.

5.1 Dataset

To fully test and evaluate our approach, we experimented on the Alzheimer's Disease Neuroimaging Initiative (ADNI) [1] dataset (Petersen et al., 2010). Alzheimer's disease (AD) is an irreversible neurodegenerative disease that results in loss of memory and mental function (thinking, planning, judgment) caused by the permanent deactivation of neuronal synapses. It is the sixth-leading cause of death in the United States and the most common cause of dementia among people over the age of 65, yet no prevention methods or cures have been discovered (Alzheimer's Association, 2018).

The ADNI was launched in 2003 as a public-private partnership, led by Principal Investigator Michael W. Weiner, MD. The primary goal of ADNI has been to test whether serial magnetic resonance imaging (MRI), positron emission tomography (PET), other biological markers, and clinical and neuropsychological assessment can be combined to measure the progression of mild cognitive impairment (MCI) and early Alzheimer's disease (AD). It has grown to include data from over 300 patients with AD, over 850 patients with mild cognitive impairment (MCI) and over 350 normal control subjects (NC).

5.1.1 Patient Selection

In our study we selected a subset of the ADNI image data which only included scans of normal (NC) and AD patients, ignoring MCI subjects to aim for the highest variance between classes. In addition, since Alzheimer's disease causes obvious damage in the brain tissue, such as shrinkage of the hippocampus and cerebral cortex and enlargement of ventricles, we utilized only the T1 MRI images available. To account for imbalance between the two classes, 58% of control subjects was randomly chosen, ending up with 152 AD patients and 101 NC subjects.

5.1.2 Preprocessing

All images downloaded from the ADNI database were already preprocessed according to the official ADNI acquisition protocol (Jack Jr et al., 2008). Additional preprocessing steps were taken to facilitate model training, such as removal of $40 - 45\%$ of the images at the beginning of the sequence and 25% at the end of the sequence, and resizing them to

---

[1]Data used in preparation of this article were obtained from the Alzheimer's Disease Neuroimaging Initiative (ADNI) database (adni.loni.usc.edu). As such, the investigators within the ADNI contributed to the design and implementation of ADNI and/or provided data but did not participate in analysis or writing of this report. A complete listing of ADNI investigators can be found at: http://adni.loni.usc.edu/wp-content/uploads/how_to_apply/ADNI_Acknowledgement_List.pdf

192×160 with Lanczos interpolation. Finally, we randomly divided the dataset into training, validation and test sets, keeping intact the sequence of each patient so that every patient appears in only one of the aforementioned sets. Table 1 shows the distribution of images (and patients) among classes.

We should note here that in our initial experiments we randomly shuffled and split all images without preserving each patient's sequences; this allowed the models to identify key features in each subject's head's morphology and achieve a perfect score on the test set (i.e. for each test set image, the model had been trained on another from the same patient). Because of this, the study of the models' generalization on new, unseen patients, which is a necessary requirement for all medical applications, became infeasible.

Table 1: Image distribution for the ADNI dataset. The respective number of patients is enclosed in parentheses.

	training	validation	test
AD	25,154 (134)	1,975 (12)	1,399 (6)
NC	24,298 (86)	2,343 (9)	2,139 (6)

5.2 Experimental Framework

In order to measure the effectiveness of the proposed methodology, the following experiment was devised:

Firstly, a Deep Neural Network architecture, capable of achieving a satisfactory performance on classifying the two categories (i.e. AD, NC), was selected. This network was trained on the aforementioned dataset with (II) and without (I) the use of traditional augmentation techniques. Afterwards, artificial images were added to the training data, forming a composite dataset, which was again used to train the same network with (IV) and without (III) the use of traditional augmentation. The four combinations are depicted in Table 2 for better clarity.

Table 2: The four experiments conducted. The use of GANs for data augmentation is represented by the horizontal axis and the use of traditional augmentation techniques on the vertical axis. The two experiments on the bottom row (i.e. III and IV) will be referred to as "composite data" experiments.

		augmentation	
		NO	YES
GAN	NO	I	II
	YES	III	IV

The goal of the study was to prove that the model trained with data augmentation through the use of GANs (III) outperforms the one without (I). Moreover, the use of GANs (III) was compared to traditional augmentation techniques (II), while the impact of both forms of augmentation (IV) was also examined.

Several metrics were used to evaluate the performance of our experiments (i.e. accuracy, precision, recall, f1), but for simplicity only the accuracy scores will be presented. Since the datasets are highly balanced, the rest of the metrics fall in line and consequently were considered redundant.

5.2.1 Classification Model

For the classification task we used the popular ResNet architecture (He et al., 2016) with 18 layers. The architecture concluded with a singe FC layer with a softmax activation function. One parameter we experimented on was the use of dropout (Srivastava et al., 2014), which was applied on FC layer; three different dropout rates were examined: 0% (which is equivalent to no dropout), 25% and 50%. Every model was trained from scratch on the available images after dataset normalization was applied. The models were trained for a total of 100 epochs with the Adam optimization algorithm (Kingma and Ba, 2014).

5.2.2 Traditional Augmentation Techniques

Due to the nature of our dataset we could only apply a limited range of visual transformations. In particular, we sequentially applied: a) horizontal flip with a given probability, b) brightness adjustment within $90\% - 110\%$ of the original values, with the same probability, c) scaling to $90\% - 110\%$ of the original size, translation by -5 to $+5$ percent per axis and rotation by -5 to $+5$ degrees, again with the same probability. Higher values for this probability correspond to larger deformations for each image. The probability will be addressed with the symbol p and will illustrate the "strength" of the augmentation. For all transformations, the discarded pixels were all padded with 0 (i.e. the intensity of the background). The whole procedure is shown in Algorithm 1. In our experiments we tried probability values (p) of 0.25 and 0.5.

Algorithm 1: Traditional augmentation algorithm.

1: **procedure** AUGMENT(img, p)
2:     **with** probability p:
3:         $img \leftarrow FlipHorizontally(img)$
4:     **with** probability p:
5:         $img \leftarrow AdjustBrightness(img, (0.9, 1.1))$
6:     **with** probability p:
7:         $img \leftarrow Scale(img, (0.9, 1.1))$
8:         $img \leftarrow Translate(img, (-5, +5))$
9:         $img \leftarrow Rotate(img, (-5, +5))$
10:     **return** img

5.2.3 GAN Augmentation

In our GAN models we used a batch size of 32, the Adam optimizer, Wasserstein loss and gradient penalty (with weight = 10 as in the original paper).

The condition upon which training was terminated required the loss of the discriminator to reach 0, at which point it is unable to distinguish between real and fake images. This was reached after around 350 epochs, as can be seen in Figure 3, which depicts the training losses of the GAN trained on the subset of ADNI control subjects (i.e. NC). The AD subset exhibited similar training loss curves.
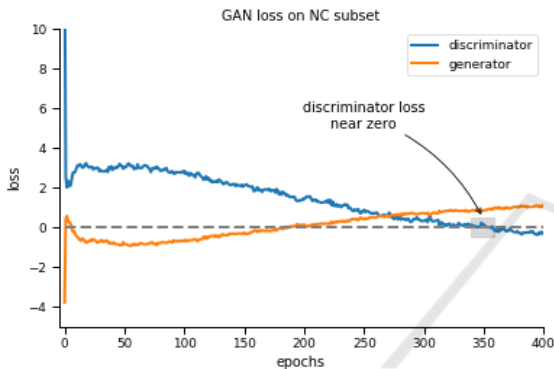
Figure 3: The loss of the GAN trained on the NC subset.

After they were fully trained, the GANs were tasked of producing 50,000 fake images for each class. These were combined with the images from the original dataset to form eight separate composite datasets, each with a different ratio of fake/real images (i.e. 25%, 50%, 75%, 100%, 125%, 150%, 175% and 200%). Table 3 shows the statistical characteristics of all eight composite training sets.

Table 3: Statistics of composite training sets for different fake/real image ratios.

	0%	25%	50%	75%
mean	35.317	35.240	35.200	35.121
std	44.920	44.826	44.783	44.709
	100%	125%	150%	175%	200%
	35.118	35.089	35.073	35.050	35.035
	44.686	44.669	44.640	44.626	44.610

The generated images impacted the statistical measures very slightly, testament of how well the GANs modeled the distribution of the training sets.

5.3 Empirical Evaluation

In this section we present a number of images produced by the trained generator in order to demonstrate

our model's potential. Most generated images proved to be of extremely high quality (Fig. 4) and showed all traits of a real MRI scan.
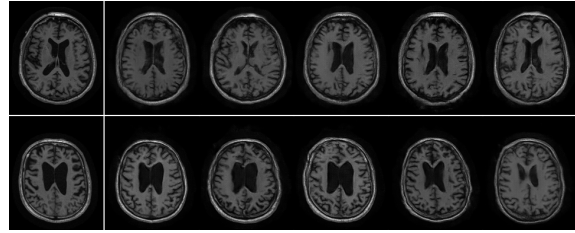
Figure 4: Comparison between real samples (leftmost images) from the two classes (NC top, AD below) and their five most lookalike GAN-created samples, in left-to-right order. The images were found using an unsupervised, 5-Nearest Neighbors model.

In Fig. 5 we demonstrate a few cases where the generator failed to synthesize meaningful images, but fortunately these mishaps constitute a very small part of our final composite data.
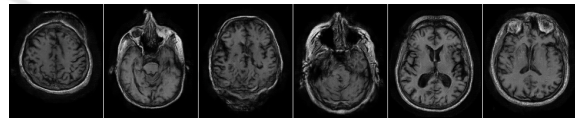

Figure 5: Some non-realistic looking samples.

Finally, with the additional assistance of a specialized radiologist, we concluded that the overall quality of the synthetic images was sufficient for use in the subsequent experiments.

6 RESULTS

Two methods were used for evaluating the results of the four experiments. The first, which we will refer to as the "runtime evaluation" involved the validation set, while the second involved the test set and is referred to as the "generalization analysis". The first was used to select the best model regarding both the epoch and hyper-parameters with which it achieves its best performance, while the second served to produce an unbiased estimate of the performance of the models.

6.1 Runtime

During training, at the end of each epoch, every model was evaluated on the validation set. This procedure was used to select the best hyper-parameters and to study the convergence of the models. The accuracy at the end of each epoch was stored for all experiments and when plotted can illustrate how the models' performance improves during training. Because of the

high oscillations some models experience, the graphs were "smoothed" through a moving average. After training, weights of the epoch at which each model achieved its highest validation accuracy were stored.

6.1.1 I. Baseline Experiments

This experiment aimed at establishing a baseline for future experiments. Three different dropout probabilities were tested, 0% (which corresponds to no dropout), 25% and 50%. The results can be seen in Figure 6.
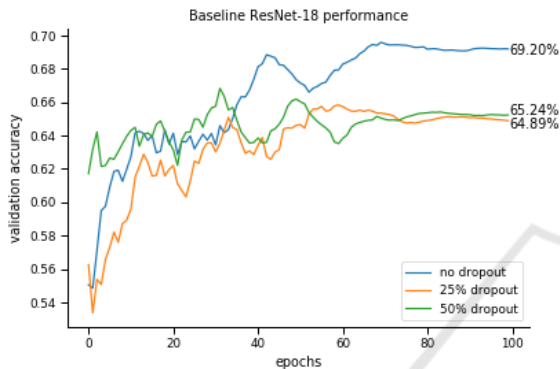

Figure 6: ResNet-18 trained on the ADNI dataset without any form of augmentation. This will be used as a baseline for the next experiments.

The best model (i.e. the ones with no dropout) achieved an accuracy of 69.2%. This will serve as the "baseline" for subsequent runs. The addition of dropout appeared to deteriorate the model's performance by around 4%.

6.1.2 II. Traditional Augmentation

After establishing the baseline, the next step was to study how the addition of traditional augmentation techniques affect the performance of the models. The augmentors used are described in Section 5.2.2. Figure 7 depicts the runtime performance of two models (i.e. one with 25% dropout probability and one without dropout) on the augmented dataset. While the model without dropout clearly outperformed the others, its use was re-evaluated during this experiment, as the regularization effect might be beneficial on not so ideal data.

While augmentation usually improves a model's performance, in the present experiment it did not, apparent by the fact that not a single model reached the baseline set by the previous experiment. One explanation could be that MR images have a very strict format. Even the mildest augmentation strategies proved counter-productive for the classification task. The
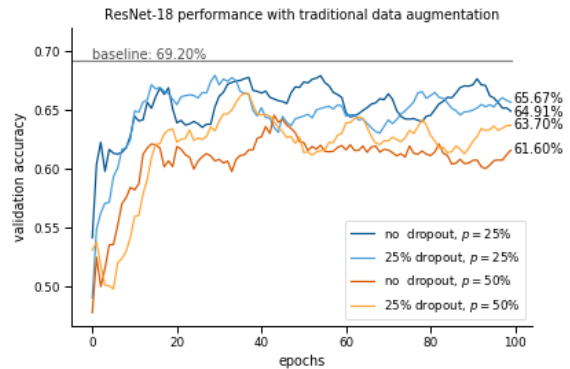
Figure 7: ResNet-18 trained on the ADNI dataset with traditional forms of augmentation. Two different network architectures were examined for two different values of p. The baseline from the previous experiment is represented by a straight line.

best model in this experiment was the one without dropout and with a 25% augmentation probability, which converged to an accuracy of 65.67%.

From the figure it is also apparent that augmentation impairs the model's convergence, evident by the heavy oscillations in the curves.

6.1.3 III. Composite Data

The main goal of this study was to evaluate the performance of a CNN trained on a dataset augmented by images generated from a GAN. In order to determine the ideal amount of artificial images to be added to the original dataset, 8 experiments were run, described in Section 5.2.3. These results are depicted in Figure 8.
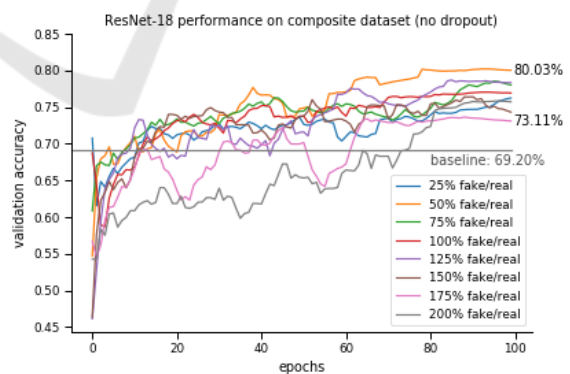

Figure 8: ResNet-18 trained on the ADNI dataset augmented with GAN generated images. 8 different datasets were used with different ratios of fake/real images. All architectures here do not make use of any dropout. The baseline is represented by a straight line.

Every single one of the runs outperforms the baseline, proving that GANs can be effectively used as data augmentors, even in tasks where traditional augmentation techniques are ineffective. The best ratio (i.e. 50%) scores more than 10% higher than the baseline.

Another thing to note is that performing data augmentation with GAN-generated images does not heavily impact the convergence of the models, as was the case with traditional augmentation techniques. Even with the increase in the size of the dataset, almost all models had converged by epoch 80. In contrast most traditional data augmentation runs (Figure 7) hadn't converged even through the full length of the experiment (100 epochs).

The optimal ratio appears to be somewhere between 50 and 125 percent; the best score was 80.03% from the model trained with a 50% fake/real ratio. Further tests were run with the use of dropout with the probability of 25%. While these were worse than those without dropout, they confirmed the best ratio. Figure 9 compares the two tests; the thick line represents the mean of all 8 scores of each test, while the error band stretches from the best to the worst.
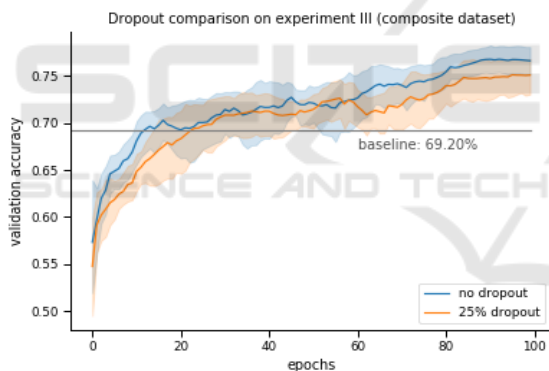
Figure 9: Each of the two tests (i.e. dropout 0% and 25%) represent 8 runs with different fake/real image ratios. The thick line follows the mean of all 8 runs, while the error band covers the distance from the best to worst model. The baseline is represented by a straight line.

Both tests score much higher than the baseline, while models that didn't use dropout outperform the others.

6.1.4 IV. Composite Data with Traditional Augmentation

Finally, the combination of both types of augmentation (i.e. traditional and GAN-based) was examined. The best model this time proved to be the one with 25% dropout and a 100% fake/real ratio, scoring 78.97%. Contrary to previous experiments, dropout

proved useful in this case. The models trained with 25% dropout, $p = 25\%$ and eight different fake/real ratios are depicted in Figure 10.
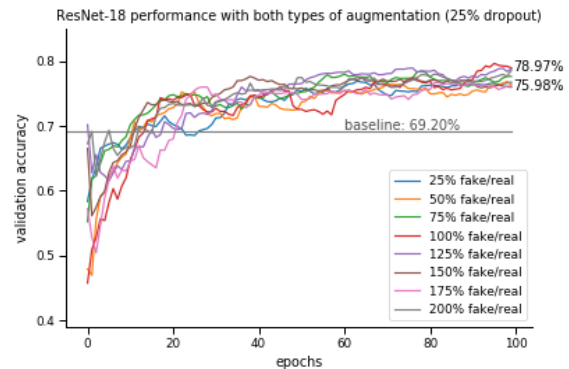

Figure 10: ResNet-18 trained on eight different composite datasets with different fake/real ratios. All models were trained with 25% dropout and $p = 25\%$. The baseline is represented by a straight line.
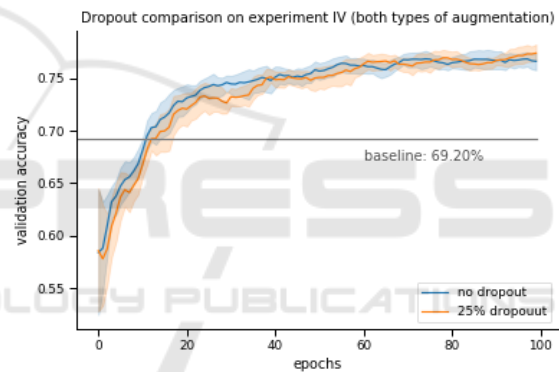

Figure 11: Each of the two tests (i.e. dropout 0% and 25%) represent 8 runs with different fake/real image ratios. The thick line follows the mean of all 8 runs, while the error band covers the distance from the best to worst model. All models are trained with a 25% dropout probability. The baseline is represented by a straight line.

The models with 25% dropout fared slightly better than the ones without, as seen in Figure 11.

Another comparison could be made involving the two experiments trained on composite datasets, i.e. one with (IV) and one without (III) the use of traditional data augmentation. Figure 12 shows the two best categories of experiments III and IV.

While the addition of traditional augmentation techniques did manage to assist in the convergence of the models, the best model was still the one from experiment III. Because there was uncertainty on whether or not the models had fully converged, their training was continued for another 100 epochs. After 200 epochs, two more models managed to reach over 80% validation accuracy: these were the models from ex-
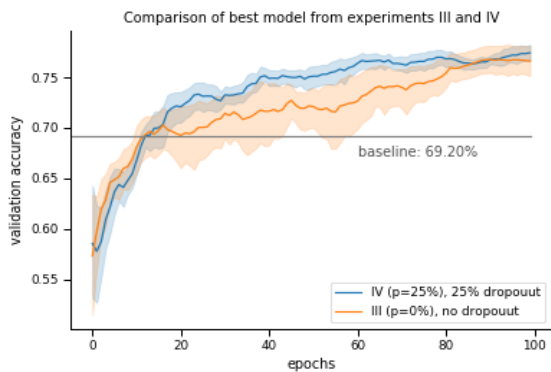
Figure 12: The best runs from experiments III and IV. The 8 runs from experiment III are without any dropout, while the 8 runs from experiment IV are with 25% dropout.

periment IV, with $p = 25\%$, a dropout probability of 25% and fake/real ratios of 125% and 150% respectively. This proves that models trained with "strong" augmentations can be effective, but require more training time.

6.2 Generalization

After training the models and evaluating them on the validation set to identify (a) the best hyper-parameters and (b) the epoch that it achieves its best performance, these "best" models were further evaluated on the test set. Because the hyper-parameter and epoch selection was done on the validation set, there is a chance that these led to an overfit of the models on that set. The test set was meant to evaluate the models one last time, as objectively as possible.

6.2.1 I. Baseline Experiments

Figure 13 shows the effect of dropout on the models trained without any form of augmentation.
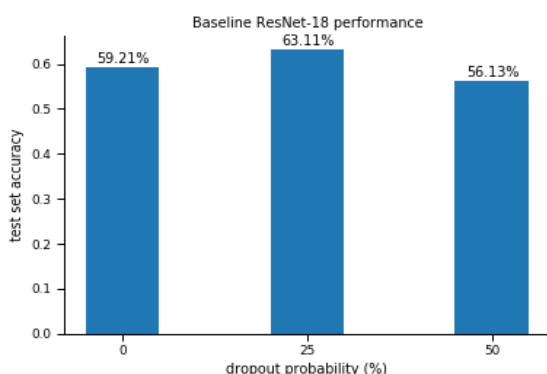
Figure 13: Three ResNet-18 architectures with different dropout probabilities were evaluated. 0% dropout is the same as not using dropout at all.

The first thing to note is that the scores are lower than the corresponding ones on the validation set, especially the one that didn't use dropout. This could be a consequence of overfitting on the validation set. In any case, the test set results are considered to be more reliable. The use of dropout appears to benefit the results on the test set, which would make sense if any overfit was taking place. The best model proved to be the one with a 25% dropout probability, which achieved an accuracy of 63.11%. This will serve as the baseline throughout the rest of the experiments.

6.2.2 II. Traditional Augmentation

The second experiment involved the use of traditional augmentation techniques; the results are shown in Figure 14.
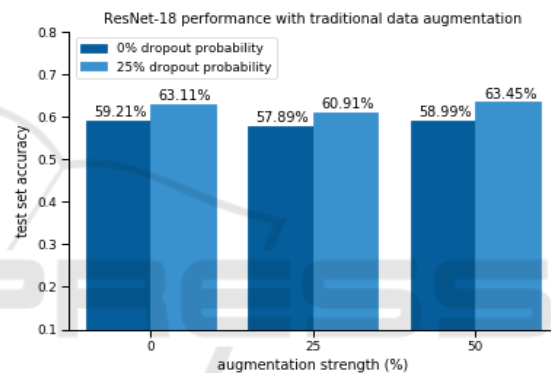

Figure 14: Two different values of p were tested (i.e. 25% and 50%). The first two bars (with $p = 0\%$) represent the previous experiment where no augmentation was used. They are considered to be the baseline.

Again, the use of dropout benefited the models, which seems to confirm our previous hypothesis of overfitting. Data augmentation appears to have little to no effect, regardless its probability. Nevertheless the best model was the one with 25% dropout probability and $p = 50\%$, with a score of 63.45%.

6.2.3 III. Composite Data

For the third experiment, the models were trained on the eight composite datasets. The results can be seen in Figure 15.

Almost all of the models that used the composite data outperformed the baseline. These results fall in line with those from Section 6.1.3. The best model was the one with a 25% dropout probability and a 50% fake/real ratio, scoring 72.81%; an increase of 15.4% over the baseline model's performance.
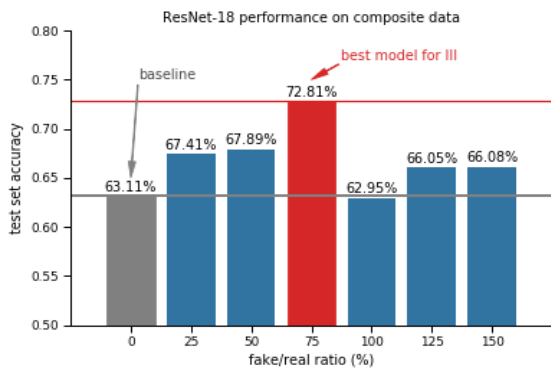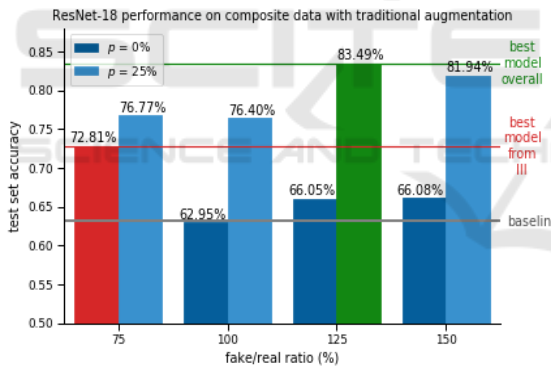
Figure 15: The models in this experiment were trained on six composite datasets with different ratios of fake/real images. Again the first one represents the accuracy scored by a model trained on the original dataset (baseline result).

6.2.4   IV. Composite Data with Traditional Augmentation

Finally, traditional augmentation techniques were used on the composite dataset. The models were evaluated with and without the use of dropout.

The results are illustrated in Figure 16.

Figure 16: The models in this experiment were trained on six composite datasets with different ratios of fake/real images. Again the first one represents the accuracy scored by a model trained on the original dataset (baseline result).

Augmentation appeared to improve the results by a large margin, in contrast to what it did in the baseline experiment. This is discussed further in Section 6.3.

The best model was the one with a 125% fake/real ratio, which achieved the best overall accuracy of 83.49%. An increase of 14.7% and 32.3% over the best model from experiment III and the baseline, respectively.

Figure 17 compares the best scoring models from each of the 4 experiments. Both models that were trained on composite datasets (i.e. III and IV), performed
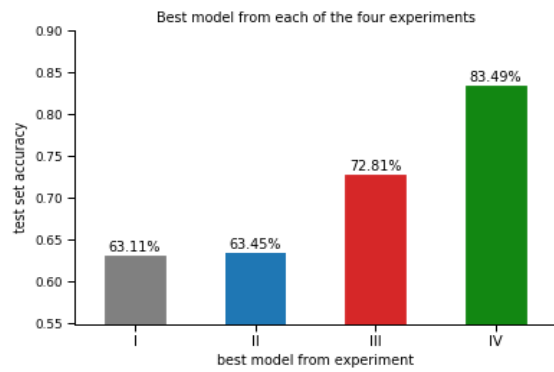

Figure 17: The best performing model from each of the four experiments is presented here. While traditional augmentation (II) didn't help the baseline model's performance (I), the use of GAN-generated images (III) did. By combining traditional and GAN augmentation schemes (IV), the best overall score was achieved.

much better than those trained on the original dataset (i.e. I and II). While traditional augmentation didn't help the baseline model (I) it did help the one trained on the composite dataset (III). A possible explanation is discussed in the following section.

6.3   Discussion

The benefit of augmenting the dataset with GAN-produced images is obvious from the experiments on both the validation (Sec. 6.1) and the test sets (Sec. 6.2). Most importantly, they increase the accuracy of the models without impacting their convergence.

The main question that arises is why does traditional data augmentation seem to work on the composite and not on the original data. A possible explanation would be that, even though the original dataset is an acceptable $50,000$ images, these were obtained from a mere 220 subjects. This results in the dataset having a low variance regarding the shapes and forms of the heads depicted in the images (i.e. the same patient will produce similar images from visit to visit). Traditional augmentation strategies would either heavily alter each image, confusing the model or, in our case, be so subtle that it simply won't improve its performance. The images introduced by GANs however don't correspond to a real patient, so each image's characteristics are unique to the dataset, increasing its variance, and thus possibly giving meaning to traditional augmentation techniques.

7   CONCLUSION

This paper presents a novel methodology for data augmentation with the use of Generative Adversarial Net-

works. It involves training a GAN for each of the classes of the original dataset and then using it to produce a number of synthetic images.

The use of a powerful generative model for producing images has many advantages over traditional augmentation schemes. The most important are the quality of the produced images and the capability of generalizing beyond the limits of the original dataset to produce new patterns. The proposed technique is especially useful in low-variance datasets where the images follow a very strict format.

To study the impact of this augmentation strategy, four experiments were conducted. First, a CNN architecture was trained on a large dataset to form a baseline (I). Afterwards the same model was trained with traditional (II) and the proposed GAN augmentation technique (III). Finally, the use of both forms of augmentation on the same dataset was examined (IV). The models were trained on MR images from the ADNI dataset to classify patients with AD from NC subjects.

The models trained with the proposed GAN augmentation methodology (III) outperform the ones with a traditional one (II) by a large margin. In fact, because of the nature of the images, the traditional techniques offered no improvement over the baseline experiment (I). The final experiment, which combined both forms of augmentation (IV) outperformed the rest, showing that while traditional augmentation could not function on its own, it synergizes well with GAN augmentation.

Because of the success of the present experiment, multiple future research directions could be spawned. An obvious choice is to experiment with different architectures for further improvements on the data quality, either within the WGAN-GP framework by utilizing a more powerful discriminator, or by using a newer, more sophisticated framework that leads to improved experimental performance, such as the Auxiliary Classifier GANs by (Odena et al., 2016) or the Progressive Growing GANs by (Karras et al., 2017).

A different research direction is to use GANs as a way to improve performance on imbalanced datasets. Instead of discarding surplus data or repeating the same images, a GAN could be trained on the least populous classes and then generate synthetic data. If trained correctly, there could be a non-trivial increase in performance.

ACKNOWLEDGEMENTS

REFERENCES

Alzheimer's Association (2018). Alzheimer's disease facts and figures. *Alzheimer's & Dementia*, 14(3):367–429.

Antoniou, A., Storkey, A., and Edwards, H. (2017). Data augmentation generative adversarial networks. *arXiv preprint arXiv:1711.04340*.

Arjovsky, M., Chintala, S., and Bottou, L. (2017). Wasserstein gan. *arXiv preprint arXiv:1701.07875*.

Bentaieb, A. and Hamarneh, G. (2018). Adversarial stain transfer for histopathology image analysis. *IEEE Transactions on Medical Imaging*, 37(3):792–802.

Ciresan, D. C., Meier, U., Gambardella, L. M., and Schmidhuber, J. (2010). Deep big simple neural nets excel on handwritten digit recognition. *CoRR*, abs/1003.0358.

Costa, P., Galdran, A., Meyer, M. I., Niemeijer, M., Abràmoff, M., Mendonça, A. M., and Campilho, A. (2018). End-to-end adversarial retinal image synthesis. *IEEE Transactions on Medical Imaging*, 37(3):781–791.

Dai, W., Doyle, J., Liang, X., Zhang, H., Dong, N., Li, Y., and Xing, E. P. (2017). SCAN: structure correcting adversarial network for chest x-rays organ segmentation. *CoRR*, abs/1703.08770.

Dar, S. U. H., Yurt, M., Karacan, L., Erdem, A., Erdem, E., and Çukur, T. (2018). Image synthesis in multi-contrast MRI with conditional generative adversarial networks. *CoRR*, abs/1802.01221.

Frangi, A. F., Tsaftaris, S. A., and Prince, J. L. (2018). Simulation and synthesis in medical imaging. *IEEE Transactions on Medical Imaging*, 37(3):673–679.

Frid-Adar, M., Diamant, I., Klang, E., Amitai, M., Goldberger, J., and Greenspan, H. (2018). Gan-based synthetic medical image augmentation for increased CNN performance in liver lesion classification. *CoRR*, abs/1803.01229.

Goodfellow, I., Pouget-Abadie, J., Mirza, M., Xu, B., Warde-Farley, D., Ozair, S., Courville, A., and Bengio, Y. (2014). Generative adversarial nets. In *Advances in neural information processing systems*, pages 2672–2680.

Gulrajani, I., Ahmed, F., Arjovsky, M., Dumoulin, V., and Courville, A. C. (2017). Improved training of wasserstein gans. *CoRR*, abs/1704.00028.

He, K., Zhang, X., Ren, S., and Sun, J. (2016). Deep residual learning for image recognition. In *Proceedings of the IEEE conference on computer vision and pattern recognition*, pages 770–778.

Hussain, Z., Gimenez, F., Yi, D., and Rubin, D. (2017). Differential data augmentation techniques for medical imaging classification tasks. In *AMIA Annual Symposium Proceedings*, volume 2017, page 979. American Medical Informatics Association.

Jack Jr, C. R., Bernstein, M. A., Fox, N. C., Thompson, P., Alexander, G., Harvey, D., Borowski, B., Britson, P. J., L. Whitwell, J., Ward, C., et al. (2008). The alzheimer's disease neuroimaging initiative (adni): Mri methods. *Journal of Magnetic Resonance Imaging: An Official Journal of the International Society for Magnetic Resonance in Medicine*, 27(4):685–691.

Karras, T., Aila, T., Laine, S., and Lehtinen, J. (2017). Progressive growing of gans for improved quality, stability, and variation. *CoRR*, abs/1710.10196.

Kingma, D. P. and Ba, J. (2014). Adam: A method for stochastic optimization. *CoRR*, abs/1412.6980.

Kukačka, J., Golkov, V., and Cremers, D. (2018). Regularization for deep learning: A taxonomy.

LeCun, Y. A., Bottou, L., Orr, G. B., and Müller, K.-R. (1998). Efficient backprop. In *Neural networks: Tricks of the trade*, pages 9–48. Springer.

Neff, T. (2018). Data augmentation in deep learning using generative adversarial networks. Master's thesis, Graz University of Technology, Graz, Austria,.

Odena, A., Olah, C., and Shlens, J. (2016). Conditional image synthesis with auxiliary classifier gans. *arXiv preprint arXiv:1610.09585*.

Perez, L. and Wang, J. (2017). The effectiveness of data augmentation in image classification using deep learning. *CoRR*, abs/1712.04621.

Petersen, R. C., Aisen, P., Beckett, L., Donohue, M., Gamst, A., Harvey, D., Jack, C., Jagust, W., Shaw, L., Toga, A., et al. (2010). Alzheimer's disease neuroimaging initiative (adni) clinical characterization. *Neurology*, 74(3):201–209.

Russakovsky, O., Deng, J., Su, H., Krause, J., Satheesh, S., Ma, S., Huang, Z., Karpathy, A., Khosla, A., Bernstein, M., Berg, A. C., and Fei-Fei, L. (2015). ImageNet Large Scale Visual Recognition Challenge. *International Journal of Computer Vision (IJCV)*, 115(3):211–252.

Shaban, M. T., Baur, C., Navab, N., and Albarqouni, S. (2018). Staingan: Stain style transfer for digital histological images. *CoRR*, abs/1804.01601.

Shin, H.-C., Tenenholtz, N. A., Rogers, J. K., Schwarz, C. G., Senjem, M. L., Gunter, J. L., Andriole, K., and Michalski, M. (2018). Medical Image Synthesis for Data Augmentation and Anonymization using Generative Adversarial Networks. *ArXiv e-prints*.

Srivastava, N., Hinton, G., Krizhevsky, A., Sutskever, I., and Salakhutdinov, R. (2014). Dropout: a simple way to prevent neural networks from overfitting. *The Journal of Machine Learning Research*, 15(1):1929–1958.

Vasconcelos, C. N. and Vasconcelos, B. N. (2017). Increasing deep learning melanoma classification by classical and expert knowledge based image transforms. *CoRR*, abs/1702.07025.

Wang, Y., Girshick, R. B., Hebert, M., and Hariharan, B. (2018). Low-shot learning from imaginary data. *CoRR*, abs/1801.05401.

Wu, R., Yan, S., Shan, Y., Dang, Q., and Sun, G. (2015). Deep image: Scaling up image recognition. *arXiv preprint arXiv:1501.02876*.

Xue, Y., Xu, T., Zhang, H., Long, L. R., and Huang, X. (2017). Segan: Adversarial network with multi-scale l_1 loss for medical image segmentation. *CoRR*, abs/1706.01805.

Yi, X., Walia, E., and Babyn, P. (2018). Generative Adversarial Network in Medical Imaging: A Review. *ArXiv e-prints*.